Atmos. Chem. Phys. Discuss., 14, 3361–3393, 2014
www.atmos-chem-phys-discuss.net/14/3361/2014/
doi:10.5194/acpd-14-3361-2014

Atmospheric Chemistry and Physics Discussions

Aerosol light-scattering enhancement due to water uptake during TCAP campaign

G. Titos[1,2], A. Jefferson[3,4], P. J. Sheridan[3], E. Andrews[3,4], H. Lyamani[1,2], L. Alados-Arboledas[1,2], and J. A. Ogren[3]

[1]Instituto Interuniversitario de Investigación del Sistema Tierra en Andalucía, IISTA-CEAMA, Universidad de Granada, Junta de Andalucía, Granada, 18006, Spain
[2]Department of Applied Physic, University of Granada, Granada, 18071, Spain
[3]Earth System Research Laboratory, National Oceanic and Atmospheric Administration, Boulder, 80305 CO, USA
[4]Cooperative Institute for Research in Environmental Sciences, University of Colorado, Boulder, 80305 CO, USA

Received: 17 January 2014 – Accepted: 28 January 2014 – Published: 5 February 2014

Correspondence to: G. Titos (gtitos@ugr.es)

Published by Copernicus Publications on behalf of the European Geosciences Union.

Abstract

Aerosol optical properties were measured by the DOE/ARM (US Department of Energy Atmospheric Radiation Measurements) Program Mobile Facility in the framework of the Two-Column Aerosol Project (TCAP) deployed at Cape Cod, Massachusetts, for a one year period (from summer 2012 to summer 2013). Measured optical properties included aerosol light-absorption coefficient (σ_{ap}) at low relative humidity (RH) and aerosol light-scattering coefficient (σ_{sp}) at low and at RH values varying from 30 to 85 %, approximately. Calculated variables included the single scattering albedo (SSA), the scattering Ångström exponent (SAE) and the scattering enhancement factor (f(RH)). Over the period of measurement, f(RH = 80 %) had a mean value of 1.9 ± 0.3 and 1.8 ± 0.4 in the PM_{10} and PM_1 fractions, respectively. Higher f(RH = 80 %) values were observed for wind directions from 0–180° (marine sector) together with high SSA and low SAE values. The wind sector from 225 to 315° was identified as an anthropogenically-influenced sector, and it was characterized by smaller, darker and less hygroscopic aerosols. For the marine sector, f(RH = 80 %) was 2.2 compared with a value of 1.8 obtained for the anthropogenically-influenced sector. The air-mass backward trajectory analysis agreed well with the wind sector analysis. It shows low cluster to cluster variability except for air-masses coming from the Atlantic Ocean that showed higher hygroscopicity. Knowledge of the effect of RH on aerosol optical properties is of great importance for climate forcing calculations and for comparison of in-situ measurements with satellite and remote sensing retrievals. In this sense, predictive capability of f(RH) for use in climate models would be enhanced if other aerosol parameters could be used as proxies to estimate hygroscopic growth. Toward this goal, we propose an exponential equation that successfully estimates aerosol hygroscopicity as a function of SSA at Cape Cod. Further work is needed to determine if the equation obtained is valid in other environments.

ACPD
14, 3361–3393, 2014

1 Introduction

The Earth's atmosphere plays an important role in the planetary energy budget through different processes that shape the Earth's climate. Changes in its composition, even in the less abundant components, like aerosols, can drive climate changes. Aerosol particles actively scatter and absorb radiation as well as change the microphysical properties of clouds. An important factor that can modify the role of aerosols in the global energy budget is the relative humidity (RH). Aerosol particles can take up water, become larger in size than their dry equivalents, and hence, scatter more light. Wet particles may also have different refractive indices and angular scattering properties than their dry counterparts. Continuous measurements of aerosol properties are typically performed under dry conditions (RH < 40 %) as recommended by international networks such as ACTRIS or GAW (WMO/GAW, 2003). These measurements at low RH can differ from what would be observed at ambient conditions and thus difficult to relate to observations of the radiative energy budget. Therefore, knowledge of the scattering enhancement due to water uptake is of great importance in order to transform dry measurements into more relevant ambient measurements, especially when comparing in-situ with remote sensing measurements (e.g., Estéve et al., 2012; Shinozuka et al., 2013) or for satellite retrievals (e.g., Wang and Martin, 2007).

The effect of RH on the aerosol light-scattering coefficient can be determined by means of a tandem nephelometer system (Covert et al., 1972; Fierz-Schmidhauser et al., 2010a, and references therein). Typically, one nephelometer measures at a reference RH (< 40 %) while the other nephelometer measures at a higher RH. The combination of both measurements allows the determination of the scattering enhancement factor, $f(\mathrm{RH})$, defined as the ratio between the scattering coefficient at high RH and the scattering coefficient at dry conditions. When these measurements are performed by scanning the higher RH over a range of values instead of at constant RH, the evaluation of $f(\mathrm{RH})$ as a function of RH is possible. Different equations have been used to fit $f(\mathrm{RH})$ vs. RH. The most widely used equation is a two-parameter, power law fit (e.g.,

ACPD
14, 3361–3393, 2014

Hänel and Zankl, 1979; Clarke et al., 2002). This equation uses a fit parameter γ to describe the humidity dependence of f(RH) for the entire RH range. The use of γ allows the comparison of measurements taken at different RH values. Carrico et al. (2003) describes several other fitting techniques as well, applied to different RH ranges.

Many studies have been published assessing the impact of RH on the aerosol light scattering coefficient for different aerosol types such as urban (Yan et al., 2009), free troposphere (Fierz-Schmidhauser et al., 2010b), continental (e.g., Sheridan et al., 2001; Pan et al., 2009) and marine aerosols (e.g., McInnes et al., 1998; Fierz-Schmidhauser et al., 2010c). Much of the recent research was performed in Central European sites (Zieger et al., 2013) and was focused on short measurement campaigns of one to three months duration. While there are a fair number of f(RH) ground based studies on a variety of aerosol types, very few of them have provided information on the aerosol scattering enhancement of fine mode aerosols; although some exceptions can be found in the literature (McInnes et al., 1998; Koloutsou-Vakakis et al., 2001; Sheridan et al., 2001; Carrico et al., 2003).

In this work, aerosol optical properties in two size ranges ($D_p < 1$ µm and $D_p < 10$ µm) were measured over a one year period at Cape Cod (Massachusetts, USA) in the framework of the Two-Column Aerosol Project (TCAP). Information concerning aerosol hygroscopicity is available for 7 months of the campaign. The main goals of this work are to characterize the hygroscopic scattering enhancement during the TCAP campaign and to explore the different situations and factors that led to changes in the hygroscopicity, as well as to explore the use of dry optical properties as proxies to estimate the hygroscopic enhancement.

ACPD
14, 3361–3393, 2014

2 Experimental site and instrumentation

2.1 Site description

The measurements presented in this study were conducted by the DOE/ARM (US Department of Energy Atmospheric Radiation Measurements) Program Mobile Facility in the framework of the Two-Column Aerosol Project (TCAP) deployed at Cape Cod, Massachusetts (Kassianov et al., 2013). Cape Cod is a peninsula jutting out into the Atlantic Ocean in the easternmost portion of the state of Massachusetts, in the northeastern United States. The deployment was located in the northeastern part of the cape (41°59′36″ N, 70°03′01″ W, 20 m a.s.l.), inside the Cape Cod National Seashore, and relatively close to large urban agglomerations such as Providence and Boston. Thus, due to its location, the site is subject to both clean and polluted conditions. The campaign started in the summer of 2012 and lasted until the summer of 2013; however, due to problems with the humidifier system, measurements of the hygroscopic enhancement are only available for approximately half of the campaign (from late September to late October 2012 and then from January to mid June 2013).

2.2 Instrumentation

Air sampling for all the instrumentation used in this study was obtained from the top of a 10 m high sampling stack of 20.3 cm in diameter. Airflow through this main stack is about 800 L min^{-1}. From this flow, 150 L min^{-1} flow through a 5.1 cm diameter stainless steel pipe in the center of this larger flow that then is divided into five 30 L min^{-1} sample lines. One of these sample lines goes to the Aerosol Observing System (AOS) instruments and the other 4 spare sample lines go out through a blower. A more detailed description of the sampling system can be found in Jefferson (2011).

The experimental set-up consists of two integrating nephelometers (TSI, model 3563) operated in series and separated by a humidifier system. The integrating nephelometer (TSI, model 3563) measures aerosol light-scattering (σ_{sp}) and hemispheric

ACPD
14, 3361–3393, 2014

backscattering (σ_{bsp}) coefficients at three wavelengths (450, 550 and 700 nm). Instrument zero checks on filtered air were automatically performed hourly. Routine maintenance and instrument calibrations with CO_2 were performed 3 times; once in July, another in January and again in June. The nephelometers are downstream of a switched impactor system which toggles the aerosol size cut between 1.0 µm (PM_1) and 10 µm (PM_{10}) aerodynamic particle diameters every 30 min. The first nephelometer measures the aerosol light-scattering coefficient at dry conditions (RH < 40 %) while the second nephelometer measures the aerosol light-scattering coefficient at a controlled RH. The humidifier consists of two concentric tubes: the inner one is a high-density porous PTFE tube and the outer tube is a stainless steel tube wrapped in a tape heater and insulation. A closed loop of water circulates between the PTFE and the outer tube. As the water temperature increases, water vapor moves through the semi-permeable PTFE membrane causing the RH of the sample air to increase. The temperature of the water is regulated via a feedback system between the downstream RH sensor, the PID (proportional-integral-derivative) controller and the heater. Temperature and relative humidity sensors (Vaisala model HMP110, accuracy of ±3 % RH) are placed throughout the system: one of the sensors is placed upstream of the impactor box and the other two sensors are placed immediately downstream of the reference and humidified nephelometers. The internal nephelometer TSI RH sensors are not used because of their slower time response and uncertainty. For this reason, the RH inside the nephelometer was calculated from the dew point temperature of the Vaisala sensor at the outlet of the humidified nephelometer and the internal nephelometer temperature. The instruments reported results at 1 Hz resolution, and the data were then averaged and recorded at 1 min resolution. The nephelometers operated at a volumetric flow rate of 30 L min^{-1}. Non-idealities due to truncation errors and the non-Lambertian light source were corrected according to Anderson and Ogren (1998). The uncertainty in the aerosol light-scattering coefficient is about 7 % (Heintzenberg et al., 2006). Every hour the RH measurement cycle started with a zero measurement and then in the humidified nephelometer the RH was increased stepwise to 80–85 % within 30 min, and

ACPD
14, 3361–3393, 2014

then decreased back to RH values of about 40 % or below during the second half of the hour. The upward RH scan corresponded to the PM_{10} size cut and the downward RH scan to PM_1. When both nephelometers measured at dry conditions (RH < 40 %) the two of them agreed well (PM_{10}: slope = 1.073 ± 0.001, intercept = 0.48 ± 0.02 Mm^{-1} and R^2 = 0.99; PM_1: slope = 0.971 ± 0.004, intercept = 0.68 ± 0.04 Mm^{-1} and R^2 = 0.77 (for the 550 nm wavelength)).

The aerosol light absorption coefficient was measured with a Particle Soot Absorption Photometer (PSAP). The method is based on the integrating plate technique in which the change in optical transmission of a filter caused by particle deposition on the filter is related to the light absorption coefficient of the deposited particles using Beer–Lambert Law. Here, a 3-wavelength version of the PSAP has been used, with nominal wavelengths of 467 nm, 531 nm, and 650 nm. The PSAP data were corrected according to Bond et al. (1999) and Ogren (2010). The uncertainty of the PSAP absorption measurement, after application of the transmission and scattering correction, is 20–30 % (Bond et al., 1999). The PSAP is also downstream of the switched impactors.

Ambient temperature, relative humidity, wind speed and direction were continuously monitored using the surface meteorological instrumentation (MET) data from the ARM AMF1 facility.

Air mass back trajectories were computed using the HYSPLIT4 model (Draxler et al., 2013) version 4.9 and were used to support the interpretation of the data.

3 Methodology

Aerosol intensive properties, such as the single scattering albedo (SSA) and scattering Ångström exponent, were calculated from the aerosol scattering and/or absorption coefficients. The aerosol single scattering albedo at 550 nm, which is the ratio of the scattering and extinction coefficients, was used in this study. The scattering Ångström exponent characterizes the wavelength dependence of σ_{sp} and was calculated using

ACPD
14, 3361–3393, 2014

the 700 nm and 450 nm wavelength pair using the following equation:

$$\mathrm{SAE}(\lambda_1 - \lambda_2) = -(\log \sigma_{sp}(\lambda_1) - \log \sigma_{sp}(\lambda_2))/(\log \lambda_1 - \log \lambda_2) \quad (1)$$

This variable increases with decreasing particle size and typically has values around 2 or higher when the scattering process is dominated by fine particles, while it is close to 0 when the scattering process is dominated by coarse particles (Delene and Ogren, 2002). In this work, both SSA(550) and SAE(450–700) refer always to dry conditions and to the PM_{10} size fraction. In order to determine SSA at 550 nm, de absorption coefficient measured with the PSAP was interpolated to the 550 nm wavelength using the above described Ångström formula.

The scattering enhancement factor $f(\mathrm{RH})$ is the ratio of $\sigma_{sp}(\lambda)$ at a high and a reference RH (λ = 550 nm in the present work):

$$f(\mathrm{RH}, \lambda) = \sigma_{sp}(\mathrm{RH}, \lambda)/\sigma_{sp}(\mathrm{dry}, \lambda) \quad (2)$$

This study uses the following two-parameter equation (Clarke et al., 2002; Carrico et al., 2003) to describe the increase in aerosol scattering due to hygroscopic growth:

$$f(\mathrm{RH}) = a\ (1 - \mathrm{RH})^{-\gamma} \quad (3)$$

where a is the intercept at RH = 0 % and γ parameterizes the magnitude of the scattering enhancement. To reduce the influence of instrument noise on the calculation, only values of the dry scattering coefficient above 5 Mm^{-1} were considered in the calculation of $f(\mathrm{RH})$. The constraints imposed for the fitting were a lower RH of 40 %, a minimum span of 30 % RH in each scan, a minimum of 50 % data coverage in each scan, the RH in the reference nephelometer had to be below 40 % and a fit R^2 value above 0.5. These criteria were applied for PM_{10} and PM_1 size fractions, with each size fraction fitted separately. A total of 2952 (PM_{10}) and 1753 (PM_1) humidograms were successfully fitted for each size respectively. Additionally, for each scan, $f(\mathrm{RH})$ values were calculated at RH = 80 % using Eq. (3), enabling comparison of scan hygroscopicity.

ACPD
14, 3361–3393, 2014

4 Results and discussion

4.1 Overview of the campaign

Figure 1 shows an overview of the daily average aerosol light-scattering and absorption coefficients, $\sigma_{sp}(550)$ and $\sigma_{ap}(531)$, single scattering albedo, SSA(550), and scattering Ångström exponent, SAE(450–700), in the PM_{10} fraction. For the entire campaign, the $\sigma_{sp}(550)$ had a mean ± standard deviation value of $22 \pm 15\,Mm^{-1}$ and the corresponding values for $\sigma_{ap}(531)$ were $1.1 \pm 0.9\,Mm^{-1}$. In general, the aerosol light absorption coefficient was very low during the measurement period, especially compared with the scattering coefficient; the SSA(550) had a mean value of 0.94 ± 0.04. On the other hand, daily-average SSA(550) values ranged from 0.77 to 1.0, denoting periods where the contribution of absorption increased. The campaign-averaged SAE(450–700) was 1.8 ± 0.6, which is quite high for a coastal environment compared with literature values (e.g., Carrico et al., 1998; Fierz-Schmidhauser et al., 2010b), and is an evidence of the high influence of anthropogenic aerosols at Cape Cod during TCAP campaign. In fact, the SAE(450–700) showed a high variability with daily values ranging from 0.6 to 3. None of the variables mentioned above showed a clear diurnal pattern, presenting very small changes throughout the day. In addition, no clear temporal trend was observed throughout the study period, although certain events of elevated $\sigma_{sp}(550)$ were observed connected with high SSA(550) values and low SAE(450–700) values. These events occurred under high wind speeds and were probably caused by sea salt particles (large particles with minimal absorption). As an example, on 9 March the $\sigma_{sp}(550)$ reached its maximum value (daily average of $84\,Mm^{-1}$). On this day the SSA had a mean value of 1 and the SAE was 0.75, suggesting that the aerosol optical properties were dominated by coarse, purely scattering particles.

Figure 2 shows the aerosol light scattering enhancement factor $f(RH = 80\,\%)$ (upper panel) and the γ parameter (lower panel) calculated for the PM_{10} and PM_1 fractions at 550 nm (hereafter the wavelength will be omitted in the notation for simplicity). Over the

ACPD
14, 3361–3393, 2014

period of measurement, $f(\mathrm{RH} = 80\,\%)$ had a mean value of 1.9 ± 0.3, with daily-mean values ranging from 1.4 to 2.6 in the PM_{10} fraction. In the PM_1 fraction, $f(\mathrm{RH} = 80\,\%)$ had a mean value of 1.8 ± 0.4 and ranged from 1.2 to 3.4. Average γ values were 0.5 for both size fractions but were relatively more variable in the PM_1 fraction (in PM_1, daily γ values ranged from 0.1 to 1.1, and in PM_{10} ranged from 0.2 and 0.9). The temporal trend of $f(\mathrm{RH} = 80\,\%)$ and γ was similar in both size fractions, however, larger differences between PM_{10} and PM_1 were observed for specific events. Specifically, on 9 March this difference was considerably larger with a mean daily $f(\mathrm{RH} = 80\,\%)$ of 3.1 in PM_1 compared to 2.4 in PM_{10}. On this day, the air mass back-trajectories arriving at 500 m a.g.l. at the measurement station were coming from the Atlantic Ocean and traveled at low altitude for the last three days, likely picking up sea salt particles. When the apparent contribution of sea salt particles (low scattering Ångström exponents and high single scattering albedos) was high, the scattering enhancement was higher in the PM_1 than in the PM_{10} fraction. Figure 3 shows the hourly $f(\mathrm{RH} = 80\,\%)$ values in PM_1 vs. $f(\mathrm{RH} = 80\,\%)$ values in PM_{10}. Data when the SAE (at dry conditions and in the PM_{10} fraction) was below and above 1, denoting a predominance of larger and smaller particles, respectively, were fitted separately. When SAE > 1 the scattering enhancement was very similar in both size fractions, however, when SAE < 1 the scattering in the PM_1 fraction experienced a higher enhancement than in the PM_{10} fraction. This same behavior was also found for the γ parameter (not shown). Zieger et al. (2013) calculated theoretical hygroscopic growth values as a function of particles size for common aerosol salts and acids. Their results showed that $f(\mathrm{RH} = 85\,\%)$ increased with decreasing particle size for all components studied, but increased more dramatically for NaCl, the largest component in sea salt.

A total of 2952 and 1753 RH scans in PM_{10} and PM_1 fractions, respectively, were fitted according to the criteria explained in Sect. 3. Additional fits were performed for the RH ranges below and above 65 %. The values of $\gamma_{>65\,\%}$ and $\gamma_{<65\,\%}$ were used to identify possible deliquescence transitions. Similar values of $\gamma_{>65\,\%}$ and $\gamma_{<65\,\%}$ indicate a monotonic growth for the entire RH range, while distinct values ($\gamma_{<65\,\%} \ll \gamma_{>65\,\%}$) in-

ACPD
14, 3361–3393, 2014

dicated no significant enhancement below 65 % and a large increase at an RH value above 65 %. For those cases in which $\gamma_{<65\%} \ll \gamma_{>65\%}$ the fit using the entire RH range underestimated f(RH) values at both low and high RH and overestimated f(RH) at the transition RH (around 65–75 % RH). To illustrate this, Fig. 4 shows the daily average humidograms for two different cases. Figure 4a shows 9 March daily average humidogram scan (γ = 0.8, $\gamma_{<65\%}$ = 0.4 and $\gamma_{>65\%}$ = 1.1) and Fig. 4b shows the daily average humidogram scan of 31 May (γ = 0.3, $\gamma_{<65\%}$ = 0.3 and $\gamma_{>65\%}$ = 0.4). On 9 March the scattering enhancement for RH > 65 % was almost three fold the enhancement for RH < 65 %. As mentioned before, during this day there was a predominance of non-absorbing coarse particles (mean SAE(450–700) = 0.75 and SSA(550) = 1), suggesting a clear contribution of sea salt particles. On 31 May the scattering enhancement was similar for both RH ranges. Slightly darker, fine mode particles dominated the aerosol on 31 May (SAE(450–700) = 1.8, SSA(550) = 0.91) compared with the previous case. In this study, fitting f(RH) to multiple RH ranges offers information on aerosol deliquescence properties.

4.2 Influence of wind speed and direction on the aerosol hygroscopicity

In order to evaluate the influence of wind speed and direction on aerosol hygroscopic properties, Fig. 5 shows f(RH = 80 %) and γ (upper panel) and SSA(550) and SAE(450–700) (lower panel) as a function of wind direction and speed. For this purpose, the hourly-average data have been averaged in bins for each 15° and 2 m s^{-1}, respectively. Both f(RH = 80 %) and γ increased with wind speed and decreased with wind direction between 0–280° and exhibited a sharp increase for wind direction between 290–360°. The SSA(550) and SAE(450–700) have opposite trends to each other, with increasing SSA(550) values and decreasing SAE(450–700) with wind speed. Similar to f(RH = 80 %), SSA(550) decreases for increasing wind direction 0–280° and shows a sharp increase from 290–360° while SAE(450–700) shows the opposite trend.

ACPD
14, 3361–3393, 2014

Figure 6 shows bivariate plots of $f(\mathrm{RH}=80\,\%)$, γ, SSA(550) and SAE(450–700) as a function of wind speed and direction (Openair software, Carslaw and Ropkins, 2012). These plots can help to better visualize the results shown in Fig. 5 and denote air mass source regions. The plots show that there is a region between approximately 225 and 315°, characterized by lower SSA(550) and higher SAE(450–700), probably influenced by anthropogenic air from the populated urban areas of Providence and Boston. In contrast, the region from 0 to 180°, characterized by higher SSA(550) and lower SAE(450–700), can be considered as marine dominated aerosols from the North Atlantic ocean. According to these results, two wind sectors have been considered for further investigation: the marine sector (0–180°) and the anthropogenically-influenced sector (225–315°). For this analysis, only wind speed values above $5\,\mathrm{m\,s^{-1}}$ were considered in order to avoid local influences. Table 1 summarizes the mean and standard deviation of the aerosol optical parameters for each sector. There is a clear difference between both wind sectors when looking at the aerosol intensive properties. The anthropogenically-influenced sector was characterized by smaller and more absorbing particles with similar $f(\mathrm{RH}=80\,\%)$ for both size fractions. Furthermore, for the anthropogenically-influenced sector, $\gamma_{>65\,\%}$ and $\gamma_{<65\,\%}$ were very similar denoting no distinct deliquescent behavior. The marine sector presented very different properties compared with the anthropogenic sector: it was characterized by larger and very weakly absorbing particles (see Table 1). The $f(\mathrm{RH}=80\,\%)$ was higher in the $\mathrm{PM_1}$ than $\mathrm{PM_{10}}$ fraction, denoting a larger scattering enhancement in the fine mode. In addition, $\gamma_{>65\,\%}$ was considerably higher (0.9 ± 0.2) than $\gamma_{<65\,\%}$ (0.4 ± 0.1), evidence of deliquescent aerosols. Carrico et al. (2000) also observed a higher scattering enhancement for clean marine conditions than for polluted situations (see Table 2) in Sagres (Portugal) which agrees with the results obtained in this section (Table 1) and those shown in Fig. 3. The $f(\mathrm{RH})$ values reported here for clean and anthropogenically influenced marine aerosols are in agreement with the range of values reported in the literature (Table 2).

ACPD
14, 3361–3393, 2014

4.3 Air-mass trajectories classification

A cluster analysis of 3 day air mass backtrajectories arriving at Cape Cod at 500 m a.g.l. at 00:00, 06:00, 12:00 and 18:00 GMT using HYSPLIT4 model (Draxler et al., 2013) version 4.9 was performed to identify the main air masses types affecting the area and their respective aerosol optical properties. This method is based on the geometric distance between individual trajectories and it takes into account speed and direction of the trajectory and height at the arriving location. A total of 1344 backward trajectories were used in the analysis. The number of clusters was selected according to the percent change in total spatial variance (TSV). Large changes in the TSV were interpreted as the merging of significantly different trajectories into the same cluster. According to this criterion, the cluster analysis resulted in five clusters of backtrajectories for air masses arriving at Cape Cod at low level. Figure 7 shows the clusters obtained with this analysis and the average humidogram for each cluster. The humidograms represent f(RH) averages in 2 % RH size bins and the error bars represent the standard deviation in the PM_{10} fraction. Table 3 shows, for each cluster, the mean and standard deviation of the optical parameters. Clusters 1–4 exhibited similar aerosol optical properties with only small differences. Cluster 5 was characterized by small SAE(450–700) and high SSA(550), as well as by high γ and f(RH = 80 %) values. The air masses included in this cluster came from the north-east, some of them originating as far away as Greenland, passing over sparsely-populated regions and the Atlantic Ocean. The high SAE(450–700) for cluster 4 together with a lower SSA(550) denotes an anthropogenic influence. Clusters 3 and 4 had similar characteristics in terms of the aerosol optical properties (see Fig. 7 and Table 3). Both clusters comprise continental air masses. Clusters 1 and 2 had hybrid properties: with a predominance of larger particles compared to clusters 3 and 4 and with higher SSA values. This is probably because the air masses in clusters 1 and 2 passed over open ocean but originated in polluted continental regions. The cluster to cluster variation in the aerosol optical properties can

ACPD
14, 3361–3393, 2014

be explained by the degree of anthropogenic and marine influence in the air masses included in each cluster.

4.4 Relationship between γ and SSA and SAE

Predictive capability and global coverage of aerosol hygroscopicity for use in climate models would be enhanced if other aerosol parameters could be used as proxies to estimate hygroscopic growth. Toward this goal, we examined covariances between γ and aerosol intensive properties. Figure 8 shows the frequency distribution of γ in the PM_{10} fraction for different SAE and SSA ranges. Values of SAE(450–700) below 1 denote a higher predominance of coarse particles and lower SSA(550) values indicate darker aerosols. From Fig. 8, it is clear that aerosols containing a higher fraction of absorbing particles (lower SSA) are less hygroscopic since the frequency distribution is shifted towards lower γ values. In contrast, Fig. 8 suggest that when coarse aerosols predominate (SAE < 1) the hygroscopic enhancement is larger. Because the γ frequency distribution segregates well between high and low values of SSA and SAE, these variables seem to be good candidates as proxies to estimate the scattering enhancement due to water uptake.

Based on the previous results, the following question arises: Can the aerosol hygroscopicity be predicted based on dry optical properties? To answer this question, Fig. 9 (upper panel) shows γ vs. SSA(550) where the color code represents the range of SAE(450–700). Figure 9a refers to γ in PM_1 and Fig. 9b refers to γ in PM_{10}. In both γ graphs, SAE(450–700) and SSA(550) corresponds to the PM_{10} size fraction and to dry conditions. The PM_1 γ was referenced to PM_{10} SSA and SAE as a means to make the fits applicable to surface measurements which may have only PM_{10} data and still differentiate the total and fine mode aerosol for models. As SSA(550) values increase the contribution of coarse particles also increases and these particles become more hygroscopic (bluish colors in Fig. 9). The increase of γ with SSA in 550 nm wavelength is well described by the following exponential functions for the PM_1 (Eq. 4) and PM_{10}

ACPD
14, 3361–3393, 2014

(Eq. 5) size fractions respectively:

$$\gamma = (3 \pm 5) \cdot 10^{-15} e^{\frac{\mathrm{SSA}}{(0.030 \pm 0.001)}} + (0.31 \pm 0.01) \quad (4)$$

$$\gamma = (4 \pm 3) \cdot 10^{-9} e^{\frac{\mathrm{SSA}}{(0.054 \pm 0.002)}} + (0.26 \pm 0.01) \quad (5)$$

The coefficient of determination was $R^2 = 0.76$ in PM_1 and $R^2 = 0.77$ in PM_{10}. The increase observed in γ for higher SSA(550) values is more pronounced in the PM_1 than in the PM_{10} size fractions. Figure 9 (lower panel) shows the frequency distribution of the residuals for the fit in PM_1 and in PM_{10}, respectively, in order to assess the quality of the regression. About 79 % of the γ values in PM_1 and 92 % in PM_{10} were estimated by the model with a difference of ±0.15 in γ. The residuals did not exhibit any dependence on SAE, suggesting that the exponential fit captures most of the covariance between SAE and SSA. The potential of this model lies in its simplicity, as the aerosol hygroscopicity can be estimated by a single parameter, the dry single scattering albedo. Quinn et al. (2005) proposed a parameterization based on the aerosol chemical composition, in particular, in the fraction of particulate organic matter to predict $f(\mathrm{RH})$. Also based on the chemical composition, Garland et al. (2007) reported that the $f(\mathrm{RH} = 80\,\%)$ varied linearly with the organic/inorganic content. However, measurements of aerosol chemical composition are commonly performed once a week and integrated over a 24 h period whereas optical properties are continuously measured at high time resolution. The exponential function presented in this study is valid for marine influenced aerosols similar to those found in Cape Cod. Further investigation is needed in order to provide a non-site dependent parameterization based on the dry optical properties.

5 Conclusions

The measured $f(\mathrm{RH})$ dependency with RH during TCAP campaign can be well described with an empirical two-parameter fit equation for both size fractions (PM_1 and PM_{10}). During the study period, $f(\mathrm{RH} = 80\,\%)$ and the fit parameter γ in PM_{10} had

ACPD
14, 3361–3393, 2014

a mean value of 1.9 and 0.5, respectively. Two distinct sectors were identified according to wind speed and direction. For the marine sector (wind speed above 5 m s^{-1} and wind direction between 0 and 180°), the γ parameter had a mean value of 0.7 ± 0.1 for $\gamma_{>65\%}$, which was considerably higher than for $\gamma_{<65\%}$. The sharp increase in f(RH) at an RH above 65 % indicated the aerosol deliquescence. The anthropogenically-influenced sector (wind speed above 5 m s^{-1} and wind direction between 225 and 315°) was characterized by a predominance of smaller and darker aerosols with lower hygroscopicity. The enhanced fine mode hygroscopic growth was more pronounced for sea salt aerosol than for mixed or anthropogenic aerosol. The air-mass trajectory classification analysis agreed with the wind sector analysis. Small differences were found between clusters, with the exception of cluster 5 that corresponds to clean marine air masses.

A clear relationship between the intensive parameters SSA and SAE with γ was observed. The γ parameter increased for increasing SSA and decreasing SAE values, that is, larger and less absorbing particles tended to be more hygroscopic. An exponential equation which fit γ to a single parameter (the single scattering albedo) was found to have a relatively low residual error, suggestion that SSA was a good proxy of the aerosol scattering hygroscopic growth. The Cape Cod study represents aerosol from a Northern Atlantic coastal site. The same analysis needs to be applied to other regions and aerosol types to catalog exponential fit parameters of γ vs. SSA over a variety of air masses. This particular study had a strong covariance between SSA and SAE, which allowed a reduction in the γ fit to a single parameter, SSA. Other sites with smoke, dust or with strong differences in aerosol composition between the fine and coarse mode may require more fit parameters.

Acknowledgements. This research was funded by the NOAA Climate Program using measurements funded by the US Department of Energy Atmospheric System Research program. The authors would like to express their gratitude to the NOAA Air Resources Laboratory (ARL) for the provision of the HYSPLIT transport and dispersion model. We would like to thank also the Openair project. G. Titos was funded by Spanish Ministry of Economy and Competitiveness – Secretariat of Science, Innovation and Development under grants BES-2011-043721

ACPD
14, 3361–3393, 2014

and EEBB-I-13-06456, and projects P10-RNM-6299, CGL2010-18782 and EU INFRA-2010-1.1.16-262254.

References

Anderson, T. L. and Ogren, J. A.: Determining aerosol radiative properties using the TSI 3563 integrating nephelometer, Aerosol Sci. Tech., 29, 57–69, 1998.

Bond, T. C., Anderson, T. L., and Campbell, D.: Calibration and intercomparison of filter-based measurements of visible light absorption by aerosols, Aerosol Sci. Tech., 30, 582–600, 1999.

Carrico, C. M., Rood, M. J., and Ogren, J. A.: Aerosol light scattering properties at Cape Grim, Tasmania, during the First Aerosol Characterization Experiment (ACE 1), J. Geophys. Res., 103, 16565–16574, 1998.

Carrico, C. M., Rood, M. J., Ogren, J. A., Neusüb, C., Wiedensohler, A., and Heintzenberg, J.: Aerosol optical properties at Sagres, Portugal during ACE-2, Tellus B, 52, 694–715, 2000.

Carrico, C. M., Kus, P., Rood, M. J., Quinn, P. K., and Bates, T. S.: Mixtures of pollution, dust, sea salt, and volcanic aerosol during ACE-Asia: radiative properties as a function of relative humidity, J. Geophys. Research., 108, 8650, doi:10.1029/2003JD003405, 2003.

Carslaw, D. C. and Ropkins, K.: Openair – an R package for air quality data analysis, Environ. Modell. Softw., 27–28, 52–61, 2012.

Clarke, A. D., Howell, S., Quinn, P. K., Bates, T. S., Ogren, J. A., Andrews, E., Jefferson, A., Massling, A., Mayol-Bracero, O., Maring, H., Savoie, D., and Cass, G.: INDOEX aerosol: a comparison and summary of chemical, microphysical, and optical properties observed from land, ship, and aircraft, J. Geophys. Res., 107, 8033, doi:10.1029/2001JD000572, 2002.

Covert, D. S., Charlson, R. J., and Ahlquist, N. C.: A study of the relationship of chemical composition and humidity to light scattering by aerosols, J. Appl. Meteorol., 11, 968–976, 1972.

Delene, D. J. and Ogren, J. A.: Variability of aerosol optical properties at four North American surface monitoring sites, J. Atmos. Sci., 59, 1135–1149, 2002.

Draxler, R. R., Stunder, B., Rolph, G., Stein, A., and Taylor, A.: HYSPLIT4 User's Guide, NOAA Air Resources Laboratory (http://www.arl.noaa.gov/documents/reports/hysplit_user_guide.pdf, last access: February 2014), 2013.

ACPD
14, 3361–3393, 2014

Esteve, A. R., Ogren, J. A., Sheridan, P. J., Andrews, E., Holben, B. N., and Utrillas, M. P.: Sources of discrepancy between aerosol optical depth obtained from AERONET and in-situ aircraft profiles, Atmos. Chem. Phys., 12, 2987–3003, doi:10.5194/acp-12-2987-2012, 2012.

Fierz-Schmidhauser, R., Zieger, P., Wehrle, G., Jefferson, A., Ogren, J. A., Baltensperger, U., and Weingartner, E.: Measurement of relative humidity dependent light scattering of aerosols, Atmos. Meas. Tech., 3, 39–50, doi:10.5194/amt-3-39-2010, 2010a.

Fierz-Schmidhauser, R., Zieger, P., Gysel, M., Kammermann, L., DeCarlo, P. F., Baltensperger, U., and Weingartner, E.: Measured and predicted aerosol light scattering enhancement factors at the high alpine site Jungfraujoch, Atmos. Chem. Phys., 10, 2319–2333, doi:10.5194/acp-10-2319-2010, 2010b.

Fierz-Schmidhauser, R., Zieger, P., Vaishya, A., Monahan, C., Bialek, J., O'Dowd, C. D., Jennings, S. G., Baltensperger, U., and Weingartner, E.: Light scattering enhancement factors in the marine boundary layer (Mace Head, Ireland), J. Geophys. Res., 115, D20204, doi:10.1029/2009JD013755, 2010c.

Garland, R. M., Ravishankara, A. R., Lovejoy, E. R., Tolbert, M. A., and Baynard, T.: Parameterization for the relative humidity dependence of light extinction: organic-ammonium sulfate aerosol, J. Geophys. Res., 112, D19303, doi:10.1029/2006JD008179, 2007.

Gassó, S., Hegg, D. A., Covert, D. S., Collins, D., Noone, K. J., Öström, E., Schmid, B., Russell, P. B., Livingston, J. M., Durkee, P. A., and Jonsson, H.: Influence of humidity on the aerosol scattering coefficient and its effect on the upwelling radiance during ACE-2, Tellus B, 52, 546–567, 2000.

Hänel, G. and Zankl, B.: Aerosol size and relative humidity: water uptake by mixtures of salts, Tellus, 31, 478–486, 1979.

Hegg, D. A., Covert, D. S., Rood, M. J., and Hobbs, P. V.: Measurements of aerosol optical properties in marine air, J. Geophys. Res., 101, D8, 12893–12903, 1996.

Heintzenberg, J., Wiedensohler, A., Tuch, T. M., Covert, D. S., Sheridan, P., Ogren, J. A., Gras, J., Nessler, R., Kleefeld, C., Kalivitis, N., Aaltonen, V., Wilhelm, R. T., and Havlicek, M.: Intercomparisons and aerosol calibrations of 12 commercial integrating nephelometers of three manufacturers, J. Atmos. Ocean. Tech., 23, 902–914, 2006.

Jefferson, A.: Aerosol Observing System (AOS) Handbook, US Department of Energy, DOE/SC-ARM/TR-014, available at: http://www.arm.gov/publications/tech_reports/handbooks/aos_handbook.pdf (last access: November 2013), 2011.

ACPD
14, 3361–3393, 2014

Kassianov, E., Barnard, J., Pekour, M., Berg, L. K., Fast, J., Michalsky, J., Lantz, K., and Hodges, G.: Temporal variability of aerosol properties during TCAP: impact on radiative forcing, Proc. SPIE, 88900O, doi:10.1117/12.2029355, 2013.

Koloutsou-Vakakis, S., Carrico, C. M., Kus, P., Rood, M. J., Li, Z., Shrestha, R., Ogren, J. A., Chow, J. C., and Watson, G.: Aerosol properties at a midlatitude Northern Hemisphere continental site, J. Geophys. Res., 106, 3019–3032, 2001.

Kotchenruther, R. A., Hobbs, P. V., and Hegg, D. A.: Humidification factors for atmospheric aerosols off the mid-Atlantic coast of the United States, J. Geophys. Res., 104, 2239–2251, 1999.

Li-Jones, X., Maring, H. B., and Propero, J. M.: Effect of relative humidity on light scattering by mineral dust aerosol as measured in the marine boundary layer over the tropical Atlantic Ocean, J. Geophys. Res., 103, 31113–31121, 1998.

McInnes, L., Bergin, M., Ogren, J. A., and Schwartz, S.: Apportionment of light scattering and hygroscopic growth to aerosol composition, Geophys. Res. Lett., 25, 513–516, 1998.

Ogren, J. A.: Comment on "Calibration and intercomparison of filter-based measurements of visible light absorption by aerosols", Aerosol Sci. Tech., 44, 589–591, 2010.

Pan, X. L., Yan, P., Tang, J., Ma, J. Z., Wang, Z. F., Gbaguidi, A., and Sun, Y. L.: Observational study of influence of aerosol hygroscopic growth on scattering coefficient over rural area near Beijing mega-city, Atmos. Chem. Phys., 9, 7519–7530, doi:10.5194/acp-9-7519-2009, 2009.

Quinn, P. K., Bates, T. S., Baynard, T., Clarke, A. D., Onasch, T. B., Wang, W., Rood, M. J., Andrews, E., Allan, J., Carrico, C. M., Coffman, D., and Wornsnop, D.: Impact of particulate organic matter on the relative humidity dependence of light scattering: a simplified parameterization, Geophys. Res. Lett., 32, L22809, doi:10.1029/2005GL024322, 2005.

Sheridan, P. J., Delene, D. J., and Ogren, J. A.: Four years of continuous surface aerosol measurements from the Department of Energy's Atmospheric Radiation Measurement Program Southern Great Plains Cloud and Radiation Testbed site, J. Geophys. Res., 106, 20735–20747, 2001.

Sheridan, P. J., Jefferson, A., and Ogren, J. A.: Spatial variability of submicrometer aerosol radiative properties over the Indian Ocean during INDOEX, J. Geophys. Res., 107, 8011, doi:10.1029/2000JD000166, 2002.

Shinozuka, Y., Johnson, R. R., Flynn, C. J., Russell, P. B., Schmid, B., Redemann, J., Dunagan, S. E., Kluzek, C. D., Hubbe, J. M., Segal-Rosenheimer, M., Livingston, J. M., Eck, T. F., Wagener, R., Gregory, L., Chand, D., Berg, L. K., Rogers, R. R., Ferrare, R. A., Hair, J. W.,

ACPD
14, 3361–3393, 2014

Hostetler, C. A., and Burton, S. P.: Hyperspectral aerosol optical depths from TCAP flights, J. Geophys. Res., 118, 12180–12194, doi:10.1002/2013JD020596, 2013.

Wang, J. and Martin, S. T.: Satellite characterization of urban aerosols: importance of including hygroscopicity and mixing state in the retrieval algorithms, J. Geophys. Res., 112, D17203, doi:10.1029/2006JD008078, 2007.

WMO/GAW: Aerosol measurement procedures guidelines and recommendations, GAWRep. 153, World Meteorol. Organ., Geneva, Switzerland, available at: ftp://ftp.wmo.int/Documents/PublicWeb/arep/gaw/gaw153.pdf (last access: February 2014), 2003.

Yan, P., Pan, X., Tang, J., Zhou, X., Zhang, R., and Zeng, L.: Hygroscopic growth of aerosol scattering coefficient: a comparative analysis between urban and suburban sites at winter in Beijing, Particuology, 7, 52–60, 2009.

Zieger, P., Weingartner, E., Henzing, J., Moerman, M., de Leeuw, G., Mikkilä, J., Ehn, M., Petäjä, T., Clémer, K., van Roozendael, M., Yilmaz, S., Frieß, U., Irie, H., Wagner, T., Shaiganfar, R., Beirle, S., Apituley, A., Wilson, K., and Baltensperger, U.: Comparison of ambient aerosol extinction coefficients obtained from in-situ, MAX-DOAS and LIDAR measurements at Cabauw, Atmos. Chem. Phys., 11, 2603–2624, doi:10.5194/acp-11-2603-2011, 2011.

Zieger, P., Fierz-Schmidhauser, R., Weingartner, E., and Baltensperger, U.: Effects of relative humidity on aerosol light scattering: results from different European sites, Atmos. Chem. Phys., 13, 10609–10631, doi:10.5194/acp-13-10609-2013, 2013.

ACPD
14, 3361–3393, 2014

Table 1. Mean and standard deviation of single scattering albedo, scattering Ångström exponent, γ parameter, $\gamma_{>65\%}$, $\gamma_{<65\%}$ and scattering enhancement factor at 80 % RH for PM_{10} fraction and scattering enhancement factor at 80 % RH for PM_1 fraction for the two wind sectors. All the variables refer to 550 nm except the scattering Ångström exponent that has been calculated between 450 and 700 nm.

Sector	SSA	SAE	γ	$\gamma_{>65\%}$	$\gamma_{<65\%}$	f(RH = 80 %)	f(RH = 80 %) in PM_1
Anthropogenic	0.93 ± 0.03	1.8 ± 0.5	0.4 ± 0.1	0.5 ± 0.2	0.4 ± 0.1	1.8 ± 0.2	1.7 ± 0.2
Marine	0.98 ± 0.02	0.9 ± 0.3	0.7 ± 0.1	0.9 ± 0.2	0.4 ± 0.1	2.2 ± 0.3	2.5 ± 0.6

ACPD
14, 3361–3393, 2014

Table 2. Hygroscopic growth factors reported in the literature for marine environments. The values of f(RH) corresponds to the ratio of the aerosol light scattering coefficients (near 550 nm wavelength) at high RH (85 % unless noted: * RH = 82 %, ** RH = 80 %) and at dry conditions (RH < 40 %). All samples were taken with size cut (D_p) of 10 µm unless specifically noted.

Source	Location	Year	f(RH)	Notes
Hegg et al. (1996a)	eastern North Pacific Ocean	1994	2.3**	No D_p cut Clean marine
Li-Jones et al. (1998)	Barbados, West Indies	1994	1.8**	Sea salt
Carrico et al. (1998)	Cape Grim, Tasmania	1995	1.98*	Clean marine
McInnes et al. (1998)	Sable Island, Canada	1996	2.7 1.7	D_p < 1 µm Marine Polluted
Kotchenruther et al. (1999)	western North Atlantic Ocean	1996	1.81** 2.30**	D_p < 4 µm "less anthropogenic" "more anthropogenic"
Carrico et al. (2000)	Sagres, Portugal	1997	1.69* 1.46* 1.86* 1.48*	D_p < 10 µm Clean Polluted D_p < 1 µm Clean Polluted
Gassó et al. (2000)	eastern North Atlantic Ocean	1997	2.0** 2.5**	D_p < 2.5 µm Polluted Clean

ACPD
14, 3361–3393, 2014

Table 2. Continued.

Source	Location	Year	f(RH)	Notes
Sheridan et al. (2002)	Indian Ocean	1999		$D_p < 1$ µm
	Indian Ocean (North)		1.55	Polluted
	Indian Ocean (Central)		1.69	Polluted
	Southern Hemisphere		2.07	Clean marine
Carrico et al. (2003)	Asia/Pacific region	2001		$D_p < 10$ µm
			2.45*	Marine
			2.24*	Polluted
				$D_p < 1$ µm
			2.95*	Marine
			2.52*	Polluted
Fierz-Schmidhauser et al. (2010b)	Mace Head, Ireland	2009	2.2	Clean
			1.8	Polluted
Zieger et al. (2011)	Cabauw, the Netherlands	2009	3	Maritime
This study	Cape Cod, MA	2012–2013		$D_p < 10$ µm
			2.2**	Clean marine
			1.8**	Anthropogenic
				$D_p < 1$ µm
			2.5**	Clean marine
			1.7**	Anthropogenic

ACPD
14, 3361–3393, 2014

Table 3. Mean and standard deviation of single scattering albedo, scattering Ångström exponent, γ parameter, $\gamma_{>65\%}$, $\gamma_{<65\%}$ and scattering enhancement factor at 80 % RH for the five clusters. All the variables refer to PM_{10} unless specifically noted and to 550 nm except the scattering Ångström exponent that has been calculated between 450 and 700 nm.

Cluster	SSA	SAE	γ	$\gamma_{>65\%}$	$\gamma_{<65\%}$	f(RH = 80 %)	f(RH = 80 %) in PM_1
1	0.94 ± 0.04	1.9 ± 0.7	0.5 ± 0.2	0.6 ± 0.3	0.4 ± 0.1	1.9 ± 0.3	1.8 ± 0.4
2	0.95 ± 0.04	1.8 ± 0.6	0.5 ± 0.1	0.5 ± 0.2	0.4 ± 0.1	1.9 ± 0.3	1.8 ± 0.3
3	0.92 ± 0.04	1.9 ± 0.5	0.4 ± 0.1	0.6 ± 0.2	0.4 ± 0.1	1.7 ± 0.2	1.6 ± 0.3
4	0.92 ± 0.03	2.1 ± 0.5	0.4 ± 0.1	0.5 ± 0.2	0.4 ± 0.1	1.8 ± 0.2	1.7 ± 0.2
5	0.97 ± 0.03	1.1 ± 0.5	0.7 ± 0.2	0.9 ± 0.2	0.4 ± 0.1	2.1 ± 0.3	2.5 ± 0.6

ACPD
14, 3361–3393, 2014

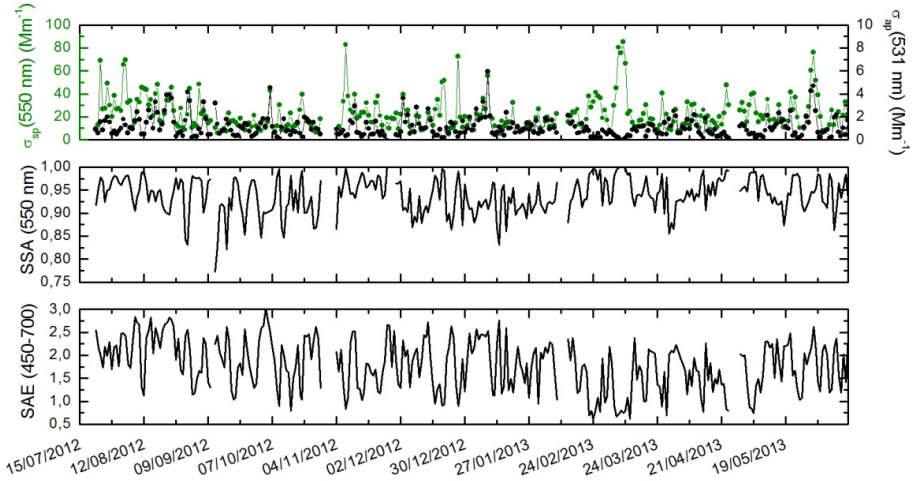

Fig. 1. Temporal evolution of the daily dry scattering and absorption coefficients (upper panel), the single scattering albedo (middle panel) and the scattering Ångström exponent (lower panel). All the parameters correspond to the PM_{10} fraction. The date is in the format dd/mm/yyyy.

ACPD
14, 3361–3393, 2014

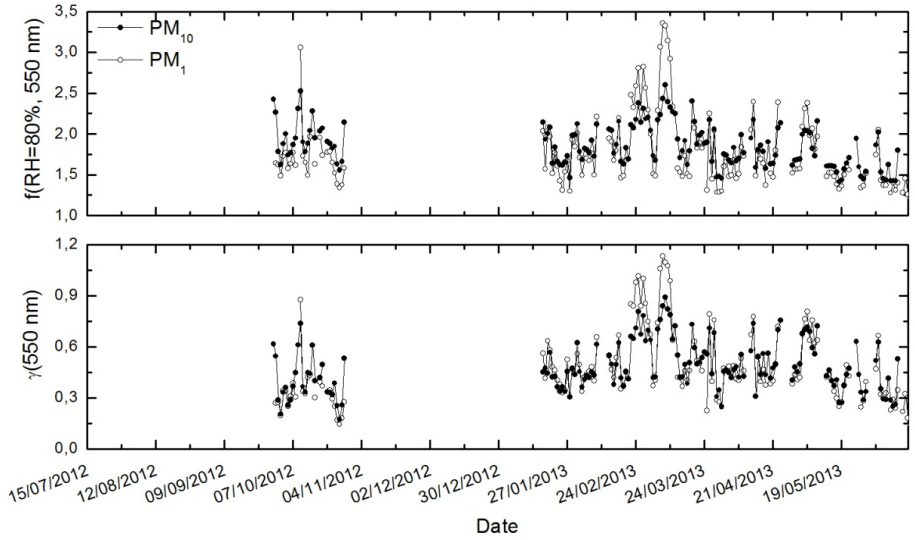

Fig. 2. Temporal evolution of the daily scattering enhancement factor at 80 % relative humidity (upper panel) and the fit parameter γ (lower panel), for PM_{10} and PM_1 fractions. The date is in the format dd/mm/yyyy.

ACPD
14, 3361–3393, 2014

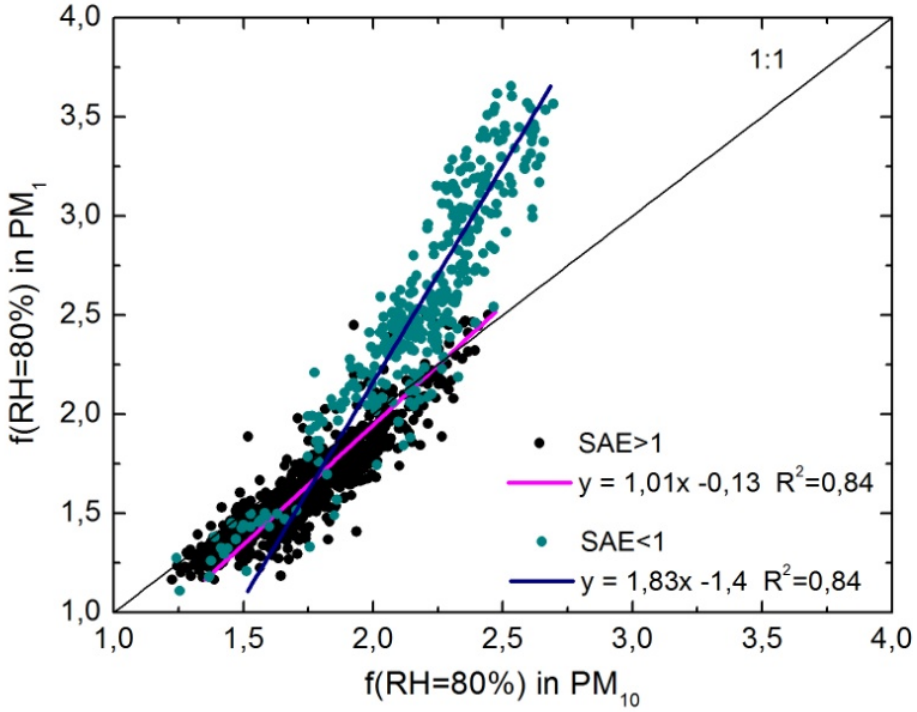

Fig. 3. Scatter plot of the hourly average scattering enhancement factors at 80 % relative humidity in the PM_1 fraction vs. the same parameter in the PM_{10} fraction. Data when the scattering Ångström exponent was below and above 1 were fitted separately.

ACPD
14, 3361–3393, 2014

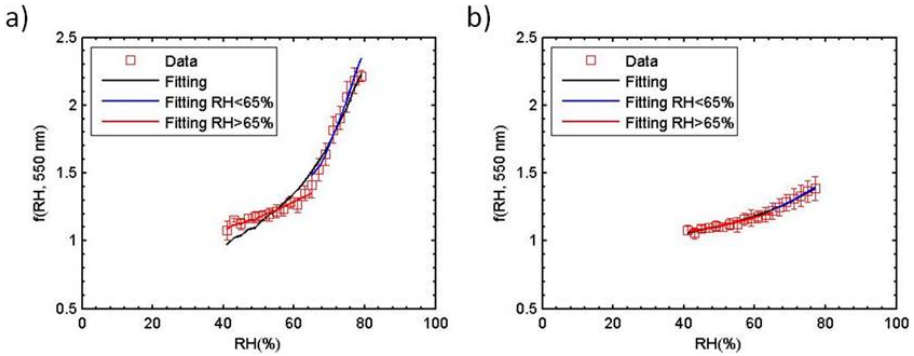

Fig. 4. Example humidograms of the scattering enhancement factor, given as daily averages where the error bars represent the standard deviation for the 9 March **(a)** and the 31 May **(b)**. The black line denotes the γ fit for the entire RH range (RH > 40 %), the blue line denotes the γ fit for RH > 65 % and the red line the γ fit for the RH < 65 %.

ACPD
14, 3361–3393, 2014

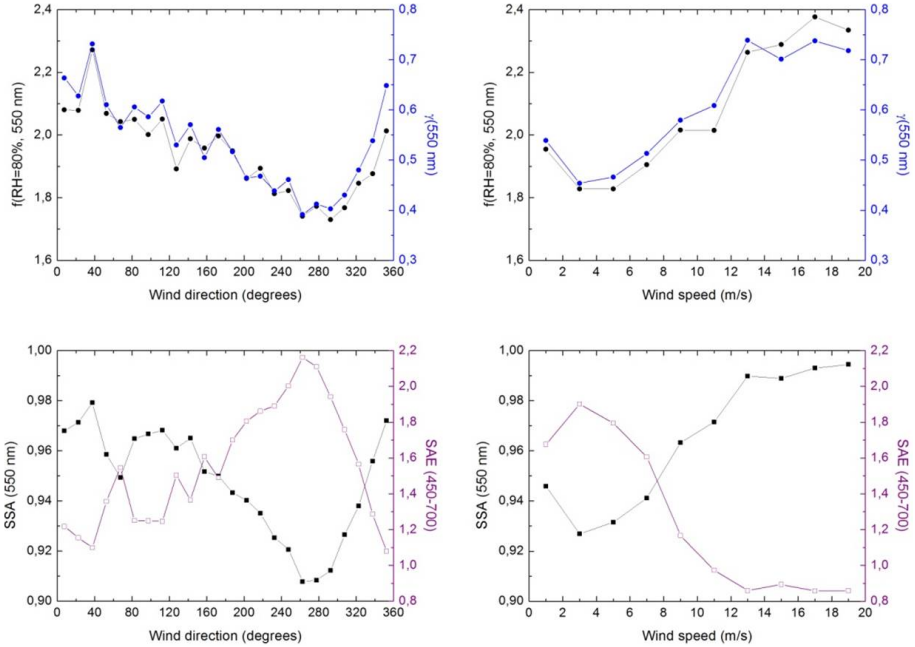

Fig. 5. Scattering enhancement factor and γ parameter (upper panel) and single scattering albedo and scattering Ångström exponent (lower panel) as a function of wind direction (left) and wind speed (right). All the variables refer to PM_{10} size fraction.

ACPD
14, 3361–3393, 2014

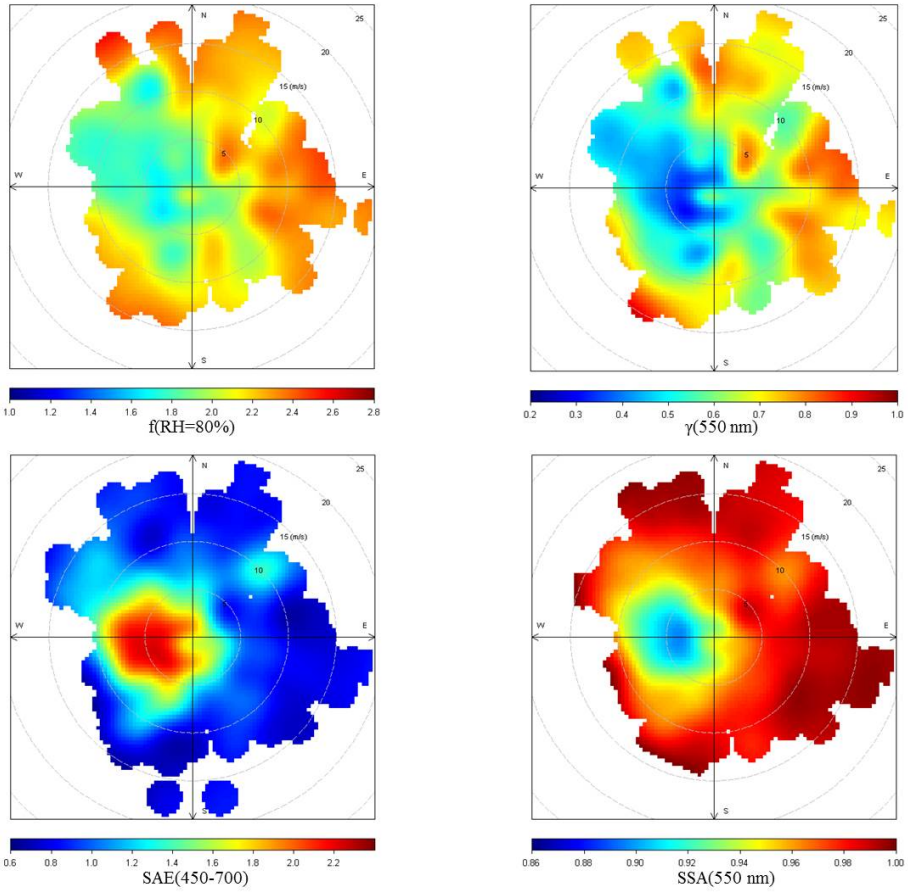

Fig. 6. Bivariate plots of the scattering enhancement factor at 80 % RH, the γ parameter, single scattering albedo and scattering Ångström exponent as a function of wind speed and direction.

ACPD
14, 3361–3393, 2014

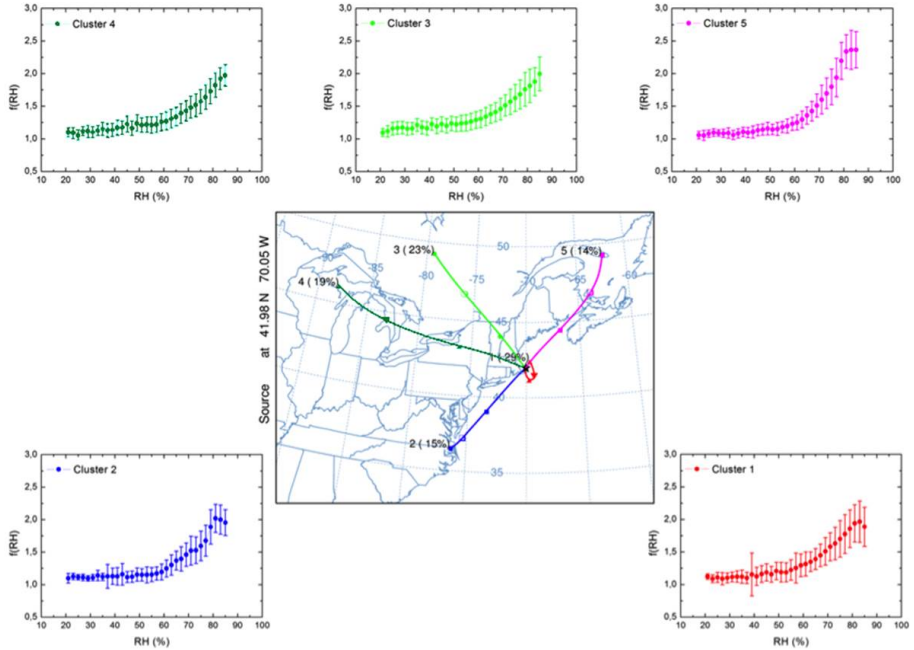

Fig. 7. Clusterization of 3 days air masses backtrajectories arriving at Cape Cod at 500 m a.g.l. at 00:00, 06:00, 12:00 and 18:00 GMT according to the HYSPLIT4 model (central panel) and average humidograms for each cluster. The error bars denote the standard deviation.

ACPD
14, 3361–3393, 2014

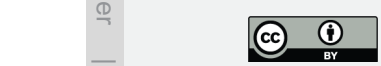

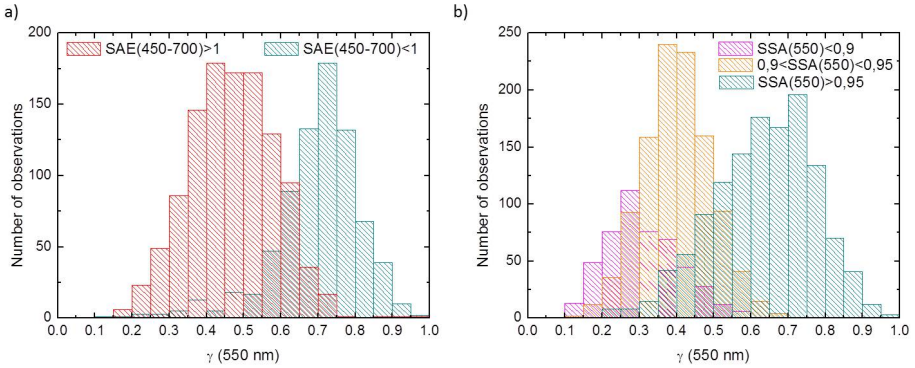

Fig. 8. Frequency distribution of the γ parameter for different scattering Ångström exponent **(a)** and single scattering albedo **(b)** ranges in the PM_{10} size fraction.

ACPD
14, 3361–3393, 2014

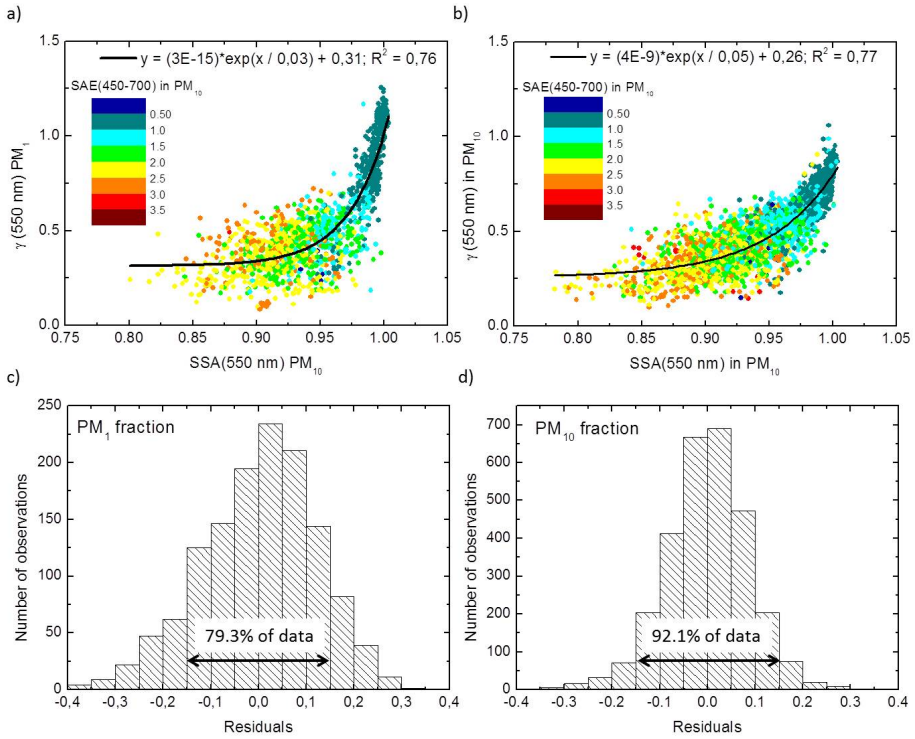

Fig. 9. γ parameter in PM_1 **(a)** and PM_{10} **(b)** vs. the single scattering albedo in PM_{10}. The color code corresponds to the scattering Ångström exponent in PM_{10}. An exponential fit has been added to the plot (black line). The residuals of these regressions are plotted as frequency distributions for PM_1 **(c)** and PM_{10} **(d)** size fractions.

ACPD
14, 3361–3393, 2014